

Evidence for Filamentarity in the Las Campanas Redshift Survey

Somnath Bharadwaj^a, Varun Sahni^b, B.S. Sathyaprakash^c, Sergei F. Shandarin^d, Capp Yess^e

^a Department of Physics and Meteorology, and, Center for Theoretical Studies, I. I. T. Kharagpur 721 302, India

^b Inter-University Centre for Astronomy & Astrophysics, Post Bag 4, Pune 411007, India

^c Department of Physics and Astronomy, Cardiff University, Cardiff, CF2 3YB, U.K.

^d Department of Physics and Astronomy, University of Kansas, Lawrence, KS 66045, USA
Theoretical Astrophysics Center, Copenhagen, Denmark

^e Department of Physical Sciences, Morehead State University, Morehead, KY 40351-1689, USA

ABSTRACT

We apply Shapefinders, statistical measures of “shape” constructed from two dimensional partial Minkowski functionals, to study the degree of filamentarity in the Las Campanas Redshift Survey (LCRS). In two dimensions, three Minkowski functionals characterise the morphology of an object, they are: its perimeter (L), area (S), and genus. Out of L & S a single dimensionless *Shapefinder Statistic*, \mathcal{F} , can be constructed ($0 \leq \mathcal{F} \leq 1$). \mathcal{F} acquires extreme values on a circle ($\mathcal{F} = 0$) and a filament ($\mathcal{F} = 1$). Using \mathcal{F} , we quantify the extent of filamentarity in the LCRS by comparing our results with a Poisson distribution with similar geometrical properties and having the same selection function as the survey. Our results unambiguously demonstrate that the LCRS displays a high degree of filamentarity both in the Northern and Southern galactic sections a result that is in general agreement with the visual appearance of the catalogue. It is well known that gravitational clustering from Gaussian initial conditions gives rise to the development of non-Gaussianity reflected in the formation of a network-like filamentary structure on supercluster scales. Consequently the fact that the smoothed LCRS catalogue shows properties consistent with those of a Gaussian random field (Colley 1997) whereas the unsmoothed catalogue demonstrates the presence of filamentarity lends strong support to the conjecture that the large scale clustering of galaxies is driven by gravitational instability.

Subject headings: Cosmology—galaxies: clustering— large scale structure of the universe: observations—methods: statistical .

1. Introduction

One of the most intriguing features of the galaxy distribution on large scales ($\gtrsim 10 h^{-1}\text{Mpc}$.) is the organisation of matter into geometrically complex structures often described as being cellular, network-like, filamentary, sheet-like, honey-comb etc (Zeldovich, Einasto & Shandarin 1982, Melott 1990, de Lapparent, Geller, & Huchra 1991, Sathyaprakash, Sahni, Shandarin & Fisher 1998). The plethora of adjectives frequently used to qualify the large scale structure of the universe underscores the difficulties inherent in trying to quantify the morphology of the galaxy distribution. This has as much to do with the need for robust statistical measures of the geometry and topology of large scale structure as it does with the virtual absence, until recently, of redshift surveys covering what may be regarded as a truly representative sample of the universe. This last gap in our knowledge has been partially filled by the Las Campanas Redshift Survey (LCRS), which for the first time appears to contain coherent structures whose size is significantly smaller than the survey size. The LCRS may therefore provide us with a statistically unbiased picture of the clustering pattern in the universe on very large scales.

Evidence for large scale connectivity and the presence of filaments, pancakes and voids also comes from semi-analytic modelling of large scale structure and from direct N-body simulations. For instance N-body simulations describing clustering from Gaussian initial conditions reveal that as a distribution evolves into the non-linear regime it begins to develop non-Gaussian features characterised by the appearance, on the one hand of large empty regions – voids, and on the other, of the concentration of matter into filaments and pancakes (Sahni & Coles 1995). The visually prominent appearance of filaments in galaxy catalogues (CfA, SSRS etc.) and in N-body simulations led to the endeavour to characterise these morphological features mathematically in order that “real filaments” might be distinguished from “apparent filaments”, the latter arising because the eye is prone to picking out structure when in fact there is none. In the process it has been shown that filamentarity is a very real feature of cosmological gravitational instability, and that the degree of filamentarity increases as gravitational clustering advances (Sathyaprakash, Sahni & Shandarin 1996, Sathyaprakash, Sahni & Shandarin 1998).

Traditionally, the clustering of galaxies in groups and clusters has been probed with some success by the two point correlation function, $\xi(r)$, which provides an estimate of the probability (in excess of random), of finding a galaxy at a distance r from another galaxy. A robust indicator of clustering, the two point correlation function nevertheless reveals very little about the morphology of the galaxy distribution, *i.e.*, the concentration of matter in sheets and/or filaments and the geometrical and topological properties of the supercluster-void distribution as a whole. The reason is simple, since $\xi(r)$ is the Fourier

transform of the power spectrum $P(k) = \langle |\delta_k|^2 \rangle$, it does not describe the build up of phase correlations which lead to the emergence of non-Gaussian features in gravitating systems arising as a result of clustering from Gaussian random initial conditions. Complete information about clustering is formally contained in the infinite hierarchy of correlation functions ξ_N , $N = 2, 3, \dots, \infty$. Although attempts have been made to calculate ξ_3 and ξ_4 , the presence of a finite number of galaxies in any sample makes the measurement of ξ_N on large scales difficult for large N . Lower order correlation functions must, therefore, be complemented by other statistical measures sensitive to geometry and topology, if we wish to probe the connectedness of large scale structure (and the associated non-Gaussianity) at a more fundamental level.

The first statistical measures to probe the geometry of large scale structure were percolation analysis and the genus curve (Zeldovich 1982, Shandarin 1983, Gott, Melott, & Dickinson 1986). When applied to N-body simulations and galaxy catalogues both methods pick out departures from Gaussianity and are helpful in discerning the presence of “network-like” and “sponge-like” features in systems undergoing gravitational clustering. The minimal spanning tree has also proved useful in quantifying geometrical features of large scale structure (Barrow, Bhavsar & Sonoda 1985). More recently, Minkowski functionals have added to our understanding of morphology (Mecke et al. 1994, Schmalzing & Buchert 1997). As demonstrated in Sahni, Sathyaprakash & Shandarin (1998), Shapefinders, a new shape diagnostic constructed out of ratios of Minkowski functionals, provides valuable information about the “shape” of a clustering pattern and can be used with considerable advantage (in conjunction with percolation analysis) to study issues relating to the morphology of large scale structure, such as the abundance of sheet-like, filament-like and ribbon-like objects. In the present paper we shall apply Shapefinders to assess the degree of filamentarity in the Las Campanas Redshift Survey.

The rest of the paper is organized as follows: Sec. 2 defines the statistics we use, Sec. 3 describes the data and the reference catalogues we deal with, finally in Sec. 4 we present our results and conclusions.

2. Minkowski Functionals and the Shapefinder Statistic

In three dimensions, the four Minkowski functionals characterising the morphology of a compact manifold are (Mecke et al. 1994): (i) its volume, V , (ii) surface area, S , (iii) the integrated mean curvature, C , and (iv) the integrated Gaussian curvature, G , (equivalently the Euler characteristic or genus). Percolation analysis can be accommodated within this scheme if one studies the behavior of the volume of the largest cluster as a function of the

filling factor for the full cluster distribution (for mass distributions clusters being defined as connected objects lying above a given density threshold). Likewise, the genus curve can be obtained if one plots G as a function of the filling factor. The Shapefinder trio is constructed out of ratios of Minkowski functionals: $L = \frac{C}{4\pi}$, $W = \frac{S}{C}$, $T = \frac{3V}{S}$. L, W & T have dimensions of length and provide an estimate of physical dimensions of an object such as its *length* L , *width* W and *thickness* T (Sahni, Sathyaprakash & Shandarin 1998). Thus $L \simeq W \simeq T$ characterises a quasispherical cluster, $L \gg W \simeq T$ a filament, $L \simeq W \gg T$ a pancake and $L \gg W \gg T$ a ribbon. Based on L, W, T a pair of dimensionless Shapefinders $\{P, F\}$ can be constructed which provide us with estimates of the planarity $P = \frac{W-T}{W+T}$ and filamentarity $F = \frac{L-W}{L+W}$ of an object, $0 \leq P, F \leq 1$. ($F = P = 0$ for a sphere, $F \simeq 1, P \simeq 0$ for a filament, $F \simeq 0, P \simeq 1$ for a pancake and $F \sim P \sim 1$ for a ribbon.)

In two dimensions the partial Minkowski functionals characterizing the morphology of a connected region are the area S , perimeter L and the number of holes in the region or genus G . The ratio $T = S/L$ characterizes the thickness of the cluster and L its extension. The ratio L/G also has dimensions of length and becomes a meaningful parameter after the onset of percolation, characterizing the scale of large scale structure (L itself obviously grows without limit after percolation with the growth of the survey size).

It appears that the Shapefinder statistic is a much better diagnostic of shape than moment-based methods, particularly when applied to topologically complex bodies such as isodensity surfaces occurring at moderate density thresholds in N-body simulations and in galaxy catalogues (Sathyaprakash, Sahni & Shandarin 1998).

In two dimensions, the Shapefinder statistic simplifies to a *single number*

$$\mathcal{F} = \frac{L^2 - 4\pi S}{L^2 + 4\pi S} \quad (1)$$

where L is the perimeter and S the area of a closed two dimensional contour. (This could be an isodensity contour in a two dimensional galaxy distribution, an isotherm of a hot/cold spot in a map of the Cosmic Microwave Background (Novikov, Feldman & Shandarin 1999), etc.) By definition $0 \leq \mathcal{F} \leq 1$; $\mathcal{F} \simeq 1$ for an ideal filament (having a finite length and zero width), and $\mathcal{F} \simeq 0$ for a circular disc.

The Las Campanas Redshift Survey contains redshifts of about 25,000 galaxies making it the largest magnitude limited three-dimensional catalogue of galaxies to date. However, the six slices into which LCRS is divided are all quasi-two-dimensional, which makes the two-dimensional shapefinder \mathcal{F} appropriate for its study.

Before applying the Shapefinder statistic to discern filamentary features in the LCRS, we shall first demonstrate its effectiveness by determining \mathcal{F} for certain eikonal shapes in

two dimensions. The first object whose shape we study is an ellipse of semi-major axis a , semi-minor axis b and eccentricity $\epsilon = \sqrt{1 - b^2/a^2}$. The area of such an ellipse is

$$S = \pi ab \quad (2)$$

and its perimeter is given by

$$L = 4aE(\epsilon) \simeq \pi(a + b) \frac{64 - 3\lambda^4}{64 - 16\lambda^2} \quad (3)$$

where $E(\epsilon) = \int_0^{\pi/2} \sqrt{1 - \epsilon^2 \sin^2 \theta} d\theta$ is the complete elliptic integral of the second kind, $\lambda = (a - b)/(a + b)$. The accuracy of (3) is better than 0.2%. In table 1 we show the value of \mathcal{F} as the ellipse is gradually deformed from an initially circular shape to a highly filamentary final shape. As pointed out in Sahni, Sathyaprakash & Shandarin (1998) other Shapefinders can also be constructed out of the Minkowski functionals S and L , a good example being provided by the transformations $\mathcal{F}' = \mathcal{F}^p$ and $\mathcal{F}'' = \sin(\pi\mathcal{F}/2)$ which define new Shapefinders from the canonical form (1). Transformations such as these can be made to define statistics that are in conformity with the visual impression of morphology of archetypal structures.

In table 1, we show results for \mathcal{F} , \mathcal{F}' (with $p = 1/2$) and \mathcal{F}'' . From the results presented in this Table, we see that the Shapefinder family \mathcal{F} , \mathcal{F}' and \mathcal{F}'' acquires continuous values between 0 and 1 as a circle is deformed into a filament, and that filamentarity is more accentuated in \mathcal{F}' and \mathcal{F}'' than in \mathcal{F} . It is interesting to contrast the behaviour of \mathcal{F} with that of the eccentricity, ϵ , another parameter characterising shape but defined *only* for an ellipse. While the value of \mathcal{F} grows in proportion to the deformation of the ellipse (and is therefore reflective of the latter’s visual shape), the change in ϵ is sudden, with the result that ϵ rapidly approaches unity even for relatively small deformations of the ellipse. Although the eccentricity is extremely good for measuring the small deviations from a circle it is clearly not the kind of behaviour one wishes to see in a “well behaved” shape-statistic which should also be sensitive to large deviations from a circle.

Next, we examine a *topologically non-trivial* object – the region between two concentric circles with radii R_1 and R_2 , $R_2 \leq R_1$ (circular disc-with-a-hole). In this case:

$$S = \pi(R_1^2 - R_2^2), \quad L = 2\pi(R_1 + R_2), \quad (4)$$

and the expression for \mathcal{F} turns out to be very simple

$$\mathcal{F} = \frac{R_2}{R_1}. \quad (5)$$

As the radius of the hole R_2 shrinks to zero, the object becomes a circular disc with $\mathcal{F} \simeq 0$, in the other extreme case when $R_1 \sim R_2$ the disc-with-a-hole reduces to a circular filament

having $\mathcal{F} \simeq 1$ (rather like the mythological serpent eating its tail). One should note that the presence of circular symmetry would lead a moment-based statistic to wrongly declare such an object as being circular or homogeneous (Sathyaprakash, Sahni & Shandarin 1998).

Results of increasing the hole size by increasing R_2 are shown in Table 2 for \mathcal{F} , \mathcal{F}' and \mathcal{F}'' . They are in broad agreement with those obtained earlier for the ellipse.

We therefore find that the two dimensional Shapefinder statistic gives sensible results when applied to both simple and topologically complicated eikonal shapes. This conclusion is supported by results obtained for three dimensional Shapefinders by Sahni et al. (1998) and Sathyaprakash, Sahni & Shandarin (1998). In this paper we shall apply \mathcal{F} to study filamentarity in the Las Camapanas Redshift Survey (the results of applying \mathcal{F}' and \mathcal{F}'' are qualitatively similar and will not be discussed separately).

3. Analysis.

3.1. The Las Camapanas Redshift Survey.

The Las Camapanas Redshift Survey (LCRS) contains approximately 25,000 galaxies with known redshifts. The survey region is divided into six slices, three each in the Northern (N_1, N_2, N_3) and Southern (S_1, S_2, S_3) Galactic hemispheres. The slices are strips of the sky 1.5° thick and 80° wide which are separated by 3° and probe a distance of up to $600 h^{-1}\text{Mpc}$. (h is the value of the Hubble parameter in units of $100 \text{ km sec}^{-1}\text{Mpc}^{-1}$). The centers of the three northern slices are at declinations -3° (N_1), -6° (N_2) and -12° (N_3), whereas the three southern slices are centered at -39° (S_1), -42° (S_2) and -45° (S_3). The survey is complete to limiting magnitude $m = 17.75$ (for more details of the LCRS survey see Shectman et al 1996).

In order to minimise selection and projection effects we apply the Shapefinder statistic to a volume limited subsample of the LCRS derived from the dense central region $200 \leq R \leq 400 h^{-1} \text{ Mpc}$. (The LCRS selection function peaks at $R \simeq 200h^{-1}\text{Mpc}$. and the region $200 \leq R \leq 400 h^{-1} \text{ Mpc}$ corresponds to the densest part of the survey.) In order to ascertain the statistical significance of our results we compare them with a statistically homogeneous two-dimensional Poisson distribution with identical selection function and geometry as the survey and corrected for projection effects (for more details, see Shandarin & Yess 1998).

Each slice is embedded in a 560×260 grid with resolution $1 h^{-1}\text{Mpc}$. This enables us to define galaxy locations on a two dimensional lattice. Lattice cells containing a galaxy are

said to be occupied or *filled*, and lattice cells with no galaxies are referred to as *empty*. The cells which lie outside the boundaries of the survey are eliminated from the lattice.

Next, we proceed to “grow” structure (or coarse-grain) by means of the following iterative procedure: At each step filled cells are made to grow isotropically (*i.e.*, in all directions) by a single unit of the mesh size. Thus any cell neighboring a filled cell (one containing a galaxy) in any of eight possible directions is also designated “filled”. This algorithm leads to the growth of filled cells at each successive iteration.

The procedure of sequentially coarse-graining a LCRS slice is shown in Figure 1 for the N1 slice. Incidentally, it also demonstrates what happens when the size of the dots in the wedge diagram plots are arbitrarily chosen. Selecting the size of the dots or the linking length one can emphasize “desired” features of the distribution such as filamentarity, connectivity, the size of the greatest supercluster or something else. So far no reason has been suggested in the literature for a particular choice of the linking length (except one corresponding to percolation transition) and therefore we use the linking length or the actual size of the dots for the purpose of parameterization.

The associated *filling factor* (FF), defined as the fraction of filled cells in the total slice, increases from a small initial value to almost unity when all the cells in the LCRS slice have inter-connected into one big all-pervading cluster. At any given value of FF (*i.e.*, at any given iterative step) we determine clusters using a friends-of-friends algorithm: any filled cell sharing a common side with another filled cell is its friend. All such “friends” define a cluster. The shape of individual clusters defined in this manner can be analysed using the Shapefinder statistic at different values of the filling factor. Large scale connectedness of galaxies in LCRS is also revealed by studying the Largest Cluster Statistics (LCS) characterizing the percolation transition as a function of the filling factor (LCS is defined as the ratio of the area of the largest cluster to the total area of all clusters, see Shandarin & Yess 1998).

It is also necessary to point out that measurements of structure in galaxy catalogues can in principle depend upon the observational strategy, particularly on the proximity of fibres mounted on a CCD. Ones intrinsic inability to pack fibres sufficiently close together in order to measure redshifts of all galaxies in a dense field might lead to the undersampling of galaxies in clusters. However since filaments are much lower density objects than clusters their detection will not be as sensitive to the spacing between fibres with the result that most of the results presented in the present paper are expected to be sufficiently robust. (For the rare case of a filament aligned along the line of sight and therefore viewed “head on” this effect could lead to undercounting of galaxies along the core of the filament and therefore weaken the signal for filamentarity. Our present estimates of filamentarity in

LCRS should therefore be treated as a lower bound to the extent of filamentarity in the “real universe”.)

3.2. Shapefinders on a grid

The Shapefinders (1) were defined for continuous contours. For contours on a grid this definition must be modified. It is easy to see that the lattice version of (1) is

$$\mathcal{F}_1 = \frac{L^2 - 16S}{L^2 + 16S} \quad (6)$$

(Note that the factor 4π in (1) has been replaced by 16 in (6).) Consider a rectangle defined on a grid with sides $n \times l$ and $m \times l$, respectively, where l is the inter-grid spacing. It is easy to see that in this case \mathcal{F}_1 reduces to

$$\mathcal{F}_1 = \frac{(n - m)^2}{(n + m)^2 + 4nm} \quad (7)$$

as a result $\mathcal{F}_1 = 0$ for $n = m$ (a square), and $\mathcal{F}_1 \rightarrow 1$ for $n \gg m$ (a filament).

It is interesting that one can define a second Shapefinder statistic which is also suitable for determining shapes of contour lines defined on a grid. Again, if l is the inter-grid spacing we have

$$\mathcal{F}_2 = \frac{L^2 - 16S}{(L - 4l)^2} \quad (8)$$

so that, for the rectangle (n, m)

$$\mathcal{F}_2 = \frac{(n - m)^2}{(n + m - 2)^2}. \quad (9)$$

We see that once more $\mathcal{F}_2 = 0$ for $n = m$ (a square), and $\mathcal{F}_2 \rightarrow 1$ for $n \gg m$ (a filament). A specific feature of \mathcal{F}_2 is that a rectangular contour of unit width $(n, 1)$ is always declared to be a filament regardless of its length n , since, substituting $m = 1$ in (9) we get $\mathcal{F}_2 = (n - 1)^2 / (n - 1)^2 = 1$.

One might question the need for introducing two separate statistics to study shapes on a lattice. The reason for this is related to the following question: Consider an “ideal” one-dimensional filament having a finite length but zero breadth. How would one go about representing this object on a grid? Depending upon how one answers this question one arrives at either \mathcal{F}_1 or \mathcal{F}_2 . One might argue that the discrete analogue of an ideal filament would be a rectangular object with width $\sim l$, (*i.e.*, width = mesh size) in which case \mathcal{F}_2

gives the correct continuum limit: $\mathcal{F}_2 = \mathcal{F} = 1$. On the other hand one might equally argue that a filament having width $< l$ is impossible to correctly define on a grid for which the Nyquist wavelength determines an effective small scale “resolution cutoff”. Therefore, if one is confined to a grid one must necessarily differentiate between objects having identical widths ($\sim l$) but varying in length, in this case the correct statistic to use is \mathcal{F}_1 .

In this paper, we report on work carried out using both \mathcal{F}_1 and \mathcal{F}_2 . As we shall show, \mathcal{F}_1 and \mathcal{F}_2 contain complementary information about filamentarity, as a result both prove to be very useful shape-diagnostics for large scale structure.

Novikov, Feldman & Shandarin 1999 used yet another approach to measuring the Minkowski functionals on a grid. Studying the 4-year COBE maps they assumed a smooth underlying field and, therefore, used a linear interpolation scheme for measuring the perimeters and areas of the clusters.

4. Results and Conclusions.

A general statistical quantity that can be constructed out of the Shapefinder \mathcal{F} is the functional $n(\mathcal{F}|A, FF)$ which describes the number density of disjoint regions of area A having given values of the filamentarity \mathcal{F} and located above a given density threshold characterised by the filling factor FF . However a good simple indicator of filamentarity is provided by the averaged quantity

$$\langle \mathcal{F}^{(d)}(FF) \rangle = \frac{\int \int n(\mathcal{F}|A, FF) \mathcal{F} A^d dA d\mathcal{F}}{\int \int n(\mathcal{F}|A, FF) A^d dA d\mathcal{F}} \quad (10)$$

describing particular moments of filamentarity in the distribution. (Each cluster of area A is identified using a nearest neighbors algorithm at a given value of the coarse-graining.)

Clearly the extent of filamentarity in a survey is strongly influenced by the morphology of its largest and most massive members: a supercluster contributes more to the overall texture of large scale structure than an individual galaxy. We therefore examine moments with $d > 1$ thereby giving greater weight to larger objects. Since our results are qualitatively similar for $d = 2, 3, 4, \dots$ we show only results for $d = 2$ and refer to the statistic $\langle \mathcal{F}^{(2)}(FF) \rangle$ simply as F . For the discrete sample under consideration (10) reduces to

$$F \equiv F_{1,2} = \frac{\sum_i A_i^2 \mathcal{F}_{1,2}^i}{\sum_i A_i^2}, \quad 0 \leq F_{1,2} \leq 1 \quad (11)$$

where the sum is evaluated at a given value of the filling factor. A_i is the area of a given

cluster and $\mathcal{F}_{1,2}^i$ is the filamentarity of the i^{th} cluster obtained by using (6) for \mathcal{F}_1 or (8) for \mathcal{F}_2 .

In Figures 2 and 3, we show the extent of filamentarity as a function of the filling factor for three northern and three southern slices of LCRS (the volume limited slice contain from 800 to 1,600 galaxies). To assess the statistical significance of our results we compare F with the corresponding quantity derived from four independent Poisson randomizations of the given LCRS slice. From Figures 2 and 3 it is clear that for moderate values of the filling factor the extent of filamentarity in *all* six slices of LCRS is *significantly greater* than in the Poisson sample. This is true for F constructed from both \mathcal{F}_1 and \mathcal{F}_2 . Comparing Fig. 2 (obtained using \mathcal{F}_1) with Fig. 3 (obtained using \mathcal{F}_2) we find that the difference between LCRS and the Poisson sample shows up at much lower filling factors for \mathcal{F}_2 . The reason for this is simple, as we demonstrated earlier, \mathcal{F}_2 is designed to be more successful in picking out smaller filaments than \mathcal{F}_1 . At low FF, small filaments appear to be much more abundant in LCRS than they are in the Poisson sample, as a result \mathcal{F}_2 easily discerns filamentarity in LCRS at small FF. Together \mathcal{F}_1 and \mathcal{F}_2 probe the extent of filamentarity over a wide range of FF.

Complementary information emphasising the “connectivity” of a distribution is revealed by percolation analysis (Shandarin & Yess 1998). At small FF each slice contains a large number of distinct clusters whose shape must be determined individually. As the FF increases, neighboring clusters begin to merge leading to a decrease in the total number of clusters in the sample and to the emergence of a single dominant “supercluster”. With increased FF we find that the largest cluster shows a very rapid increase in size as a result of which it soon spans the entire survey region. This corresponds to the onset of percolation. We determine \mathcal{F} for individual clusters and the area of the largest cluster at each level of coarse graining. As $FF \rightarrow 1$ the percolating supercluster fills the entire slice, the value of \mathcal{F} then drops to a small value which describes the shape of the survey region. (If the slice were an exact square the value \mathcal{F} would approach 0 as $FF \rightarrow 1$.) In Fig. 4 we plot the Largest Cluster Statistic (LCS is the fractional size of the largest cluster relative to all clusters at a given value of coarse graining) against FF (the fraction of filled cells in the total area of the slice). Comparing these results with those of the Poisson distribution we clearly see that the growth in the largest cluster is more rapid in LCRS than it is in the randomized catalogue (constructed with the same selection function and number of galaxies and therefore having identical geometrical properties to LCRS) confirming the earlier results of Shandarin and Yess (1998).

To summarise we have shown that clustering of galaxies in LCRS is significantly non-Gaussian: it is dominated by filaments and its global geometry is network-like (in the

parlance of Shandarin & Yess 1998). Our analysis also indicates that Shapefinders recognize non-Gaussian features in LCRS at lower filling factors than the percolation curve and that Shapefinders and percolation analysis supplement each other in discerning the geometrical properties of the galaxy distribution on large scales.

Finally we note that at $FF \sim 1$ the extent of filamentarity in LCRS declines (from a value close to unity) and becomes smaller than in the Poisson catalogue. The decrease in F in both LCRS and the Poisson catalogue is simply due to the fact that all clusters in the sample have now merged into a single “super-duper” cluster which resembles a quasi-homogeneous object with several holes (empty regions). Such an object when probed using the Shapefinder statistic appears very filamentary both in LCRS and the Poisson sample. However as $FF \rightarrow 1$ the holes gradually get filled and F drops to a small value which describes the shape of the survey region. We do not attach much significance to results shown in Fig.2 and Fig.3 at $FF > 0.6$ because at such large values of the filling factor the percolating supercluster spans the entire sample region. As a result at large FF some geometrical properties of the supercluster begin to be progressively determined by the size and geometry of the sample volume and cease to be reflective of the (formally infinite) galaxy distribution from which the finite sample is drawn.

The largest cluster in two dimensions can be characterized by two parameters: the thickness of the cluster wall separating nearby voids $T = S/L$ and the length of the cluster boundary per void $L/|G|$. The cluster perimeter L itself is not a good measure because for the percolating cluster it diverges as the area of the survey grows without bound. On the other hand the parameter $L/|G|$ defined for the percolating cluster proves to be remarkably stable over a wide range of linking lengths. Fig. 5 shows the length of the cluster boundary per void ($L/|G|$) as a function of wall thickness (S/L) for both the LCRS and reference catalogues. The stability of the statistic $L/|G|$ is reflected by the fact that while the thickness of the supercluster grows by a factor of three from $\approx 5 h^{-1}\text{Mpc}$ to $\approx 16 h^{-1}\text{Mpc}$ the mean value of $L/|G|$ decreases only marginally: from $\approx 110 h^{-1}\text{Mpc}$ to $\approx 70 h^{-1}\text{Mpc}$ in the LCRS catalogue. The structure in the reference Poisson catalogues is of considerably smaller size than in the LCRS. This is reflective of the existence of large scale structure in the galaxy distribution marked by a percolating network of filaments separating large voids.

Although Fig. 5 gives the scale of the structure, we wish to stress that it is not the diameter of the empty cells seen in Fig. 1. The parameter $L/|G|$ has a meaning of “length of the supercluster contour line per void”. In our case the mean number of voids is large: about 30 in the LCRS and about 130 in the randomized catalogues (at wall thickness of $\approx 10 h^{-1}\text{Mpc}$). This allows us to say that the sample is sufficiently large and the average diameter of the voids (at thickness $\approx 10 h^{-1}\text{Mpc}$) is about $80/\pi \approx 25 h^{-1}\text{Mpc}$. (Large

values of $|G|$ for a given cluster indicate a large number of holes and consequently a greater porosity of the cluster. This applies particularly to the percolating supercluster for which G can be very large and negative.)

It is interesting to note that an analysis of LCRS using the genus curve has shown that at large values of the smoothing radius, LCRS reveals statistical properties which are consistent with those of a Gaussian random field (Colley 1997). Our results on the other hand (and those of Shandarin & Yess 1998) show that the *unsmoothed* LCRS catalogue displays strongly non-Gaussian features. In this context, it is worthwhile to reiterate that N-body gravitating systems clustering from Gaussian initial conditions rapidly develop non-Gaussian features reflected both in a network-like structure and by a growth of filamentarity in the morphology of clusters and superclusters (Sathyaprakash, Sahni & Shandarin 1996, Sahni, Sathyaprakash & Shandarin 1997, Sathyaprakash, Sahni & Shandarin 1998). The effects of smoothing such a distribution on large scales would be to add greater weight to the clustering of long range modes still in the linear regime, and hence statistically distributed in the manner of a Gaussian random field (Dominik & Shandarin 1992, Sahni & Coles 1995). When viewed in this context the results of this paper (and those of Shandarin & Yess 1998), together with the results of Colley (1997), appear to provide strong support for the scenario in which the large scale structure of the universe evolved via gravitational clustering from Gaussian initial conditions predicted (for instance) by Inflationary Models of the very early universe.

Acknowledgements. S. Shandarin acknowledges the support of NSF-EPSCoR grant, GRF grant at the University of Kansas and from TAC Copenhagen. We wish to thank an anonymous referee for comments that led to an improvement in the manuscript.

REFERENCES

- Barrow, J.D., Bhavsar, S.P. & Sonoda D.H. 1985, MNRAS 216, 17.
- Colley, W.N. 1997, ApJ 489, 471.
- de Lapparent, V., Geller, M.J. & Huchra, J.P. 1991, ApJ, 369, 273.
- Dominik, K. & Shandarin, S.F. 1992, ApJ, 393, 450.
- Gott, J.R., Melott, A.L. & Dickinson, M. 1986, ApJ, 306, 341.
- Mecke, K.R., Buchert, T. & Wagner, H., 1994, Astron. Astrophys., 288, 697.
- Melott, A.L. 1990, Physics Reports, 193, 1.

- Novikov, D.I., Feldman, H. & Shandarin, S.F. 1999, *Int. J. of Mod. Phys. D*, 8, 291
- Sahni, V. & Coles, P., 1995, *Physics Reports*, 262, 1.
- Sahni, V., Sathyaprakash, B.S. & Shandarin, S.F. 1997, *ApJ* 476, L1.
- Sahni, V., Sathyaprakash, B.S. & Shandarin, S.F. 1998, *ApJ* 495, L5.
- Sathyaprakash, B.S., Sahni, V. & Shandarin, S.F. 1996, *ApJ*, 462, L5.
- Sathyaprakash, B.S., Sahni, V., Shandarin, S.F. and Fisher, K. 1998, *ApJ*, 507, L109.
- Sathyaprakash, B.S., Sahni, V. & Shandarin, S.F. 1998, *ApJ* 508, 551.
- Schmalzing, J. & Buchert, T. 1997, *ApJ* 482, L1.
- Shandarin, S.F. 1983, *Soviet Astron. Lett.*, 9, 104.
- Shandarin, S. and Yess, C. 1998, *ApJ*, 505, 12.
- Shectman, S.A., Landay, S.D., Oemler, A., Tucker, D.L., Kirshner, R.P., Lin, H. and Schechter, P.L. 1996, *Wide-Field Spectroscopy and the Distant Universe, Proceedings of the 35th Herstmonceux Conference*, eds. S.J. Maddox and A. Aragon-Salamanca, World Scientific, Singapore.
- Zeldovich, Ya. B. 1982, *Soviet Astron. Lett.*, 8, 102.
- Zeldovich, Ya. B., Einasto, J. & Shandarin, S.F. 1982, *Nature*, 300, 407.

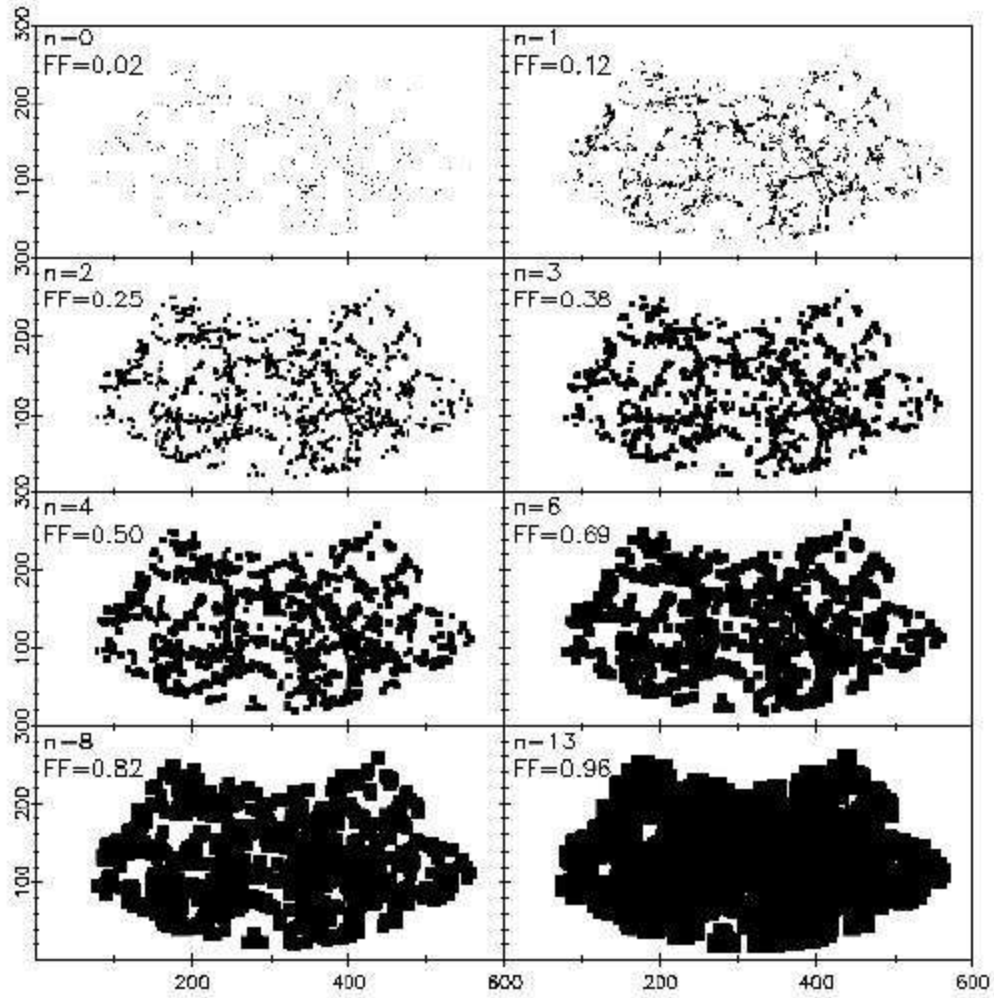


Fig. 1.— The first Northern LCRS slice shown at different values of coarse-graining (n). The value of the filling factor (FF) at each level of coarse-graining is also shown. Here $n = 0$ shows galaxies in the original N_1 slice without coarse graining. The axis units are h^{-1} Mpc.

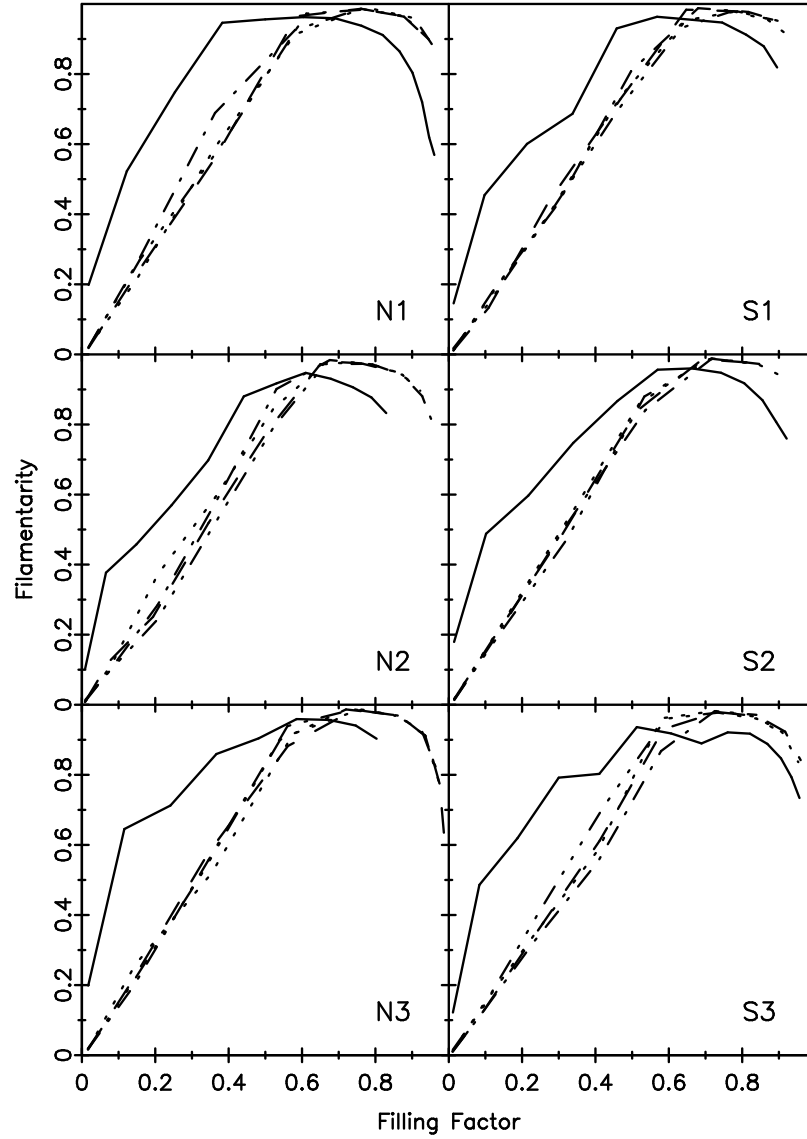


Fig. 2.— The filamentarity statistic F is shown plotted against the filling factor FF for each slice in the LCRS (solid line). For comparison we also show F for four independent random Poisson fields for each of the slices (dashed and dotted lines). The shape-statistic F shown here is constructed from the discrete Shapefinder \mathcal{F}_1 .

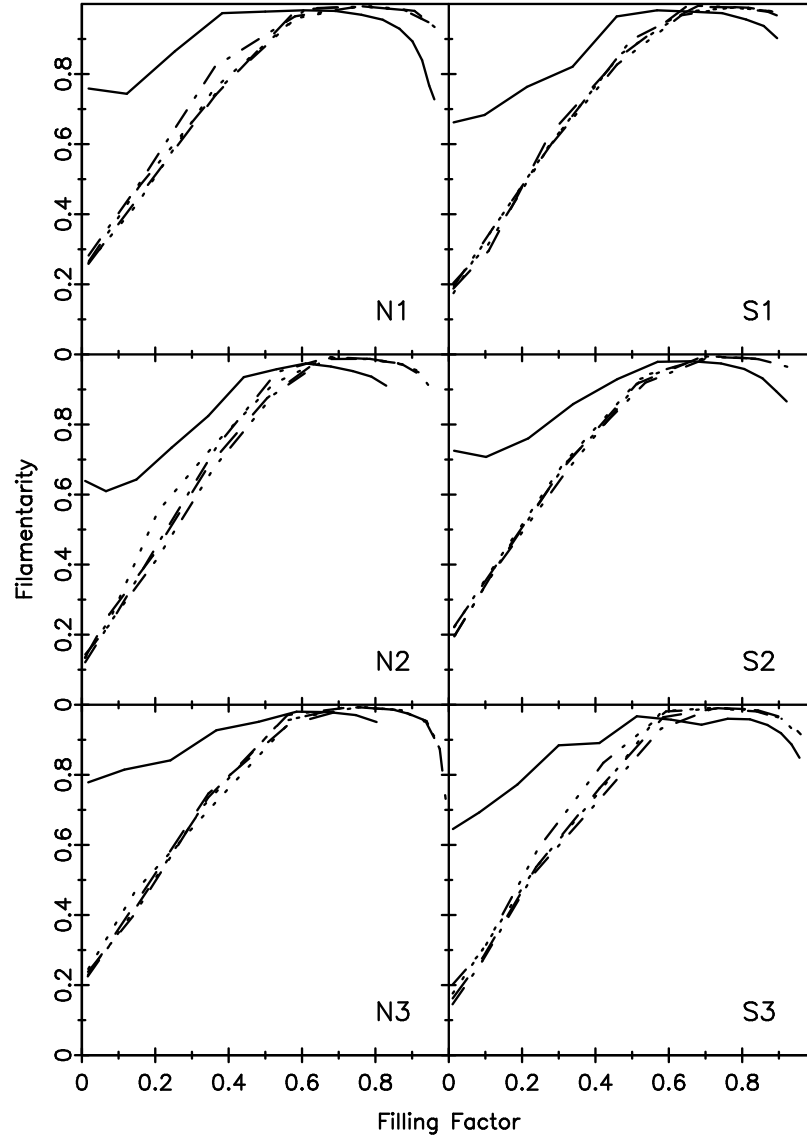


Fig. 3.— The filamentarity statistic F is shown plotted against the filling factor FF for each slice in the LCRS (solid line). For comparison we also show F for four independent random Poisson fields for each of the slices (dashed,dotted lines). The shape-statistic F shown here is constructed from the discrete Shapfinder \mathcal{F}_2 .

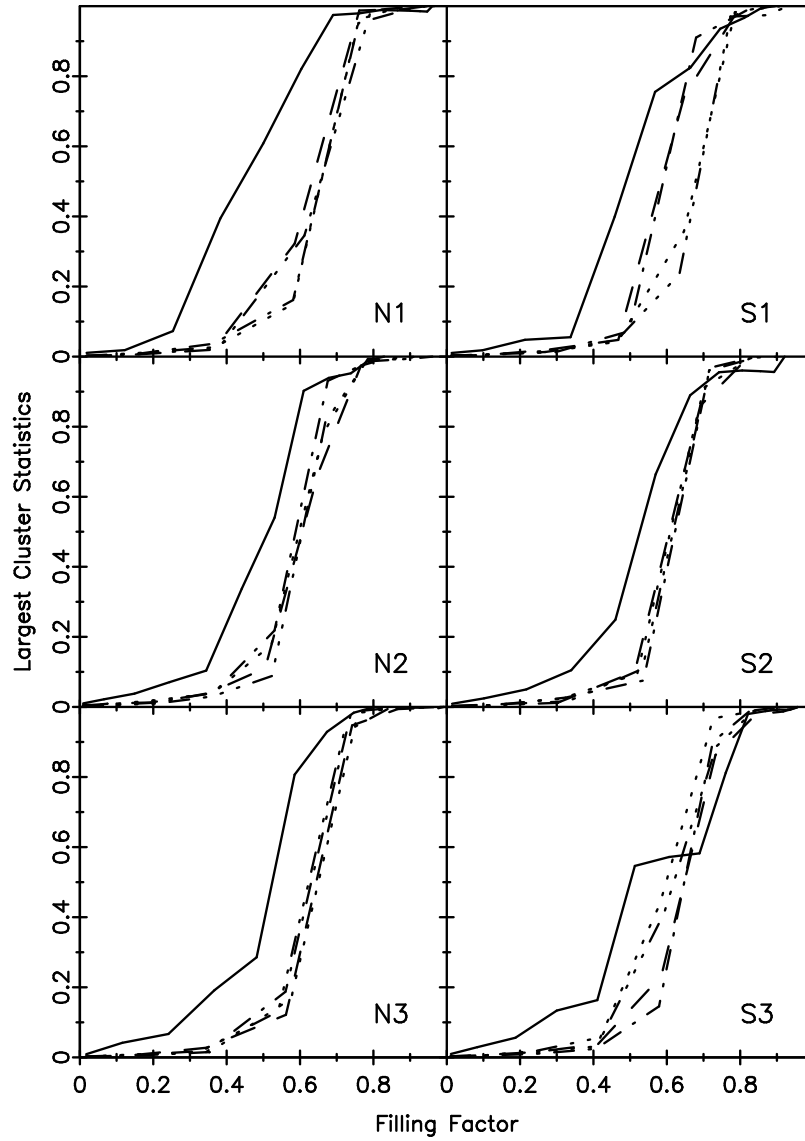


Fig. 4.— The largest cluster statistics (LCS) is shown plotted against the filling factor FF for each slice in the LCRS (solid line). For comparison we also show (LCS) for four independent random Poisson fields for each of the slices (dashed,dotted lines).

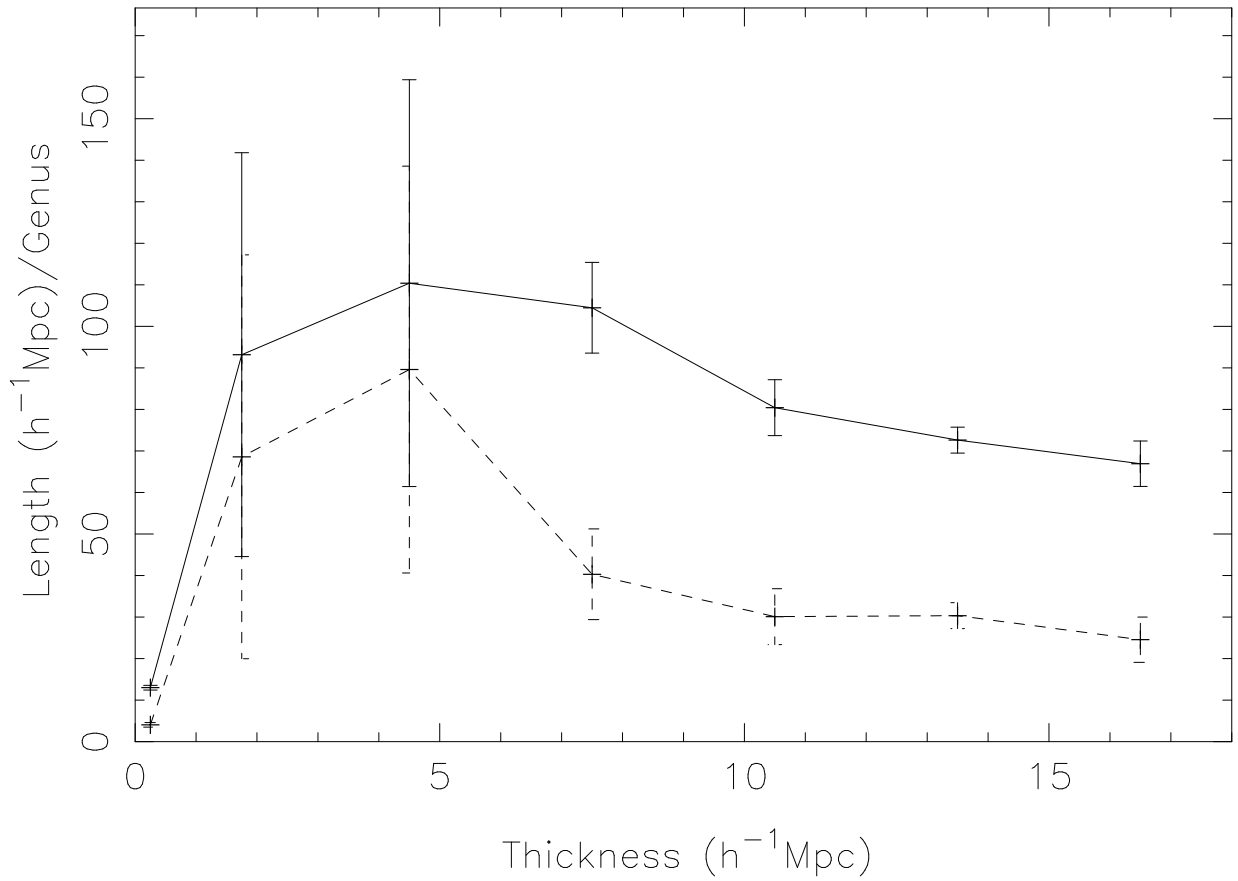


Fig. 5.— The solid curve shows the ratio length/genus of the largest cluster plotted as a function of the thickness of the largest cluster. The values of the thickness from the different slices have been divided into bins of $3h^{-1}$ Mpc and the average value of the length/genus in each bin has been plotted as the solid curve. The error-bars show $1 - \sigma$ fluctuations. For comparison we have shown the same quantity for the random Poisson fields using dashed lines.

Table 1: Shapefinders \mathcal{F} , \mathcal{F}' & \mathcal{F}'' describe the shape of an ellipse having semi-major axis a , semi-minor axis b and eccentricity ϵ .

a/b	ϵ	\mathcal{F}	$\mathcal{F}' = \mathcal{F}^{1/2}$	$\mathcal{F}'' = \sin(\pi\mathcal{F}/2)$
1	0	0	0	0
3	0.94	0.20	0.45	0.31
5	0.98	0.38	0.62	0.56
10	0.99	0.61	0.78	0.82

Table 2: Shapefinders \mathcal{F} , \mathcal{F}' & \mathcal{F}'' describe the shape of the region between two concentric circles with radii R_1 & R_2 (circular disc-with-a-hole).

R_1, R_2	\mathcal{F}	$\mathcal{F}' = \mathcal{F}^{1/2}$	$\mathcal{F}'' = \sin(\pi\mathcal{F}/2)$
10, 0	0	0	0
10, 2	0.20	0.45	0.31
10, 4	0.40	0.63	0.59
10, 6	0.60	0.77	0.81
10, 8	0.80	0.89	0.95
10, 9	0.90	0.95	0.99